


ORIGINAL RESEARCH

# Binge Alcohol Exposure in Adolescence Impairs Normal Heart Growth

Lizhuo Ai, MS; Edith Perez, MS; AnnaDorothea Asimes, PhD; Theerachat Kampaengsri, BS; Maxime Heroux, PhD; Andrei Zlobin, PhD; Mark A. Hiske, BS; Charles S. Chung, PhD; Toni R. Pak, PhD; Jonathan A. Kirk , PhD

**BACKGROUND:** Approximately 1 in 6 adolescents report regular binge alcohol consumption, and we hypothesize it affects heart growth during this period.

**METHODS AND RESULTS:** Adolescent, genetically diverse, male Wistar rats were gavaged with water or ethanol once per day for 6 days. In vivo structure and function were assessed before and after exposure. Binge alcohol exposure in adolescence significantly impaired normal cardiac growth but did not affect whole-body growth during adolescence, therefore this pathology was specific to the heart. Binge rats also exhibited signs of accelerated pathological growth (concentric cellular hypertrophy and thickening of the myocardial wall), suggesting a global reorientation from physiologic to pathologic growth. Binge rats compensated for their smaller filling volumes by increasing systolic function and sympathetic stimulation. Consequently, binge alcohol exposure increased PKA (protein kinase A) phosphorylation of troponin I, inducing myofilament calcium desensitization. Binge alcohol also impaired in vivo relaxation and increased titin-based cellular stiffness due to titin phosphorylation by PKC $\alpha$  (protein kinase C  $\alpha$ ). Mechanistically, alcohol inhibited extracellular signal-related kinase activity, a nodal signaling kinase activating physiology hypertrophy. Thus, binge alcohol exposure depressed genes involved in growth. These cardiac structural alterations from binge alcohol exposure persisted through adolescence even after cessation of ethanol exposure.

**CONCLUSIONS:** Alcohol negatively impacts function in the adult heart, but the adolescent heart is substantially more sensitive to its effects. This difference is likely because adolescent binge alcohol impedes the normal rapid physiological growth and reorients it towards pathological hypertrophy. Many adolescents regularly binge alcohol, and here we report a novel pathological consequence as well as mechanisms involved.

**Key Words:** aging ■ alcohol ■ myocardial structure ■ myofilament protein

Approximately 1 in 6 adolescents report regular binge alcohol consumption,<sup>1,2</sup> a pattern of drinking that elevates blood alcohol content (BAC) to 0.08 g/dL within 2 hours. Considering the size of the population consuming alcohol at these levels, it is essential that we determine the effects on the growing adolescent heart. It is already known that alcohol can interfere with normal brain development that occurs during adolescence.<sup>3–6</sup> While the basic structure and number of cardiomyocytes is cemented early in development, the rapid enlargement in body weight and surface area during adolescence<sup>7</sup> requires a

concurrent rise in cardiac output to meet the increased metabolic demands. Thus, the heart must grow during this period<sup>8–11</sup> through postnatal physiological cellular hypertrophy. During the course of adolescence, these processes can increase heart mass by  $\geq 2$ -fold,<sup>12</sup> which could make this period particularly vulnerable to the cardiovascular effects of alcohol. However, the direct physiological effects of adolescent binge alcohol consumption on the growing heart, in either humans or animal models, are unknown.

Prior studies in middle-aged and older individuals<sup>13</sup> and recently in young adults<sup>14</sup> show that slow,

Correspondence to: Jonathan A. Kirk, PhD, Department of Cell and Molecular Physiology, Loyola University Chicago Stritch School of Medicine, Center for Translational Research, Room 522, 2160 South First Avenue, Maywood, IL 60153. Email: [jkirk2@luc.edu](mailto:jkirk2@luc.edu)

Supplementary Materials for this article are available at <https://www.ahajournals.org/doi/suppl/10.1161/JAHA.119.015611>

For Sources of Funding and Disclosures, see page 11.

© 2020 The Authors. Published on behalf of the American Heart Association, Inc., by Wiley. This is an open access article under the terms of the Creative Commons Attribution-NonCommercial-NoDerivs License, which permits use and distribution in any medium, provided the original work is properly cited, the use is non-commercial and no modifications or adaptations are made.

JAHA is available at: [www.ahajournals.org/journal/jaha](http://www.ahajournals.org/journal/jaha)

## CLINICAL PERSPECTIVE

### What Is New?

- One in 6 adolescents report regular binge alcohol consumption, but its effects on the growing adolescent heart are unknown.
- Using a physiologically relevant rat model, we found that binge alcohol consumption inhibits normal cardiac growth and reorients it towards pathological hypertrophy.
- Mechanistically, alcohol inhibited cardiomyocyte extracellular signal-related kinase activity and depressed genes involved in growth, as well as sarcomere function and response to stress.

### What Are the Clinical Implications?

- While further evidence is required to determine whether these findings translate to human adolescents, they suggest a serious pathology that may go unnoticed and is likely to have long-term consequences on cardiovascular health.
- Adolescent binge alcohol consumption may need to be considered as a significant risk factor for the development of cardiovascular disease.

## Nonstandard Abbreviations and Acronyms

|                               |  |
|-------------------------------|--|
| <b>ANP</b>                    | atrial natriuretic peptide               |
| <b>BAC</b>                    | blood alcohol content                    |
| <b>ERK1/2</b>                 | extracellular signal-related kinase      |
| <b>LV</b>                     | left ventricular                         |
| <b>LVEDV</b>                  | left ventricular end-diastolic volume    |
| <b>LVPWd</b>                  | left ventricular posterior wall diameter |
| <b>MHC</b>                    | myosin heavy chain myosin heavy chain    |
| <b>PND</b>                    | postnatal day                            |
| <b>PKA</b>                    | protein kinase A                         |
| <b>PKC<math>\alpha</math></b> | protein kinase C $\alpha$                |
| <b>SL</b>                     | sarcomere length                         |

progressive adverse remodeling occurs with sustained alcohol consumption that can eventually result in alcoholic cardiomyopathy. Alcoholic cardiomyopathy is characterized by a dilated left ventricle, normal or slightly increased left ventricular (LV) wall thickness, increased LV mass, and reduced ejection fraction.<sup>15,16</sup> However, the effects of alcohol on the heart may be different across the lifespan, so previous studies in adults may not translate to adolescents. Indeed, we hypothesize that binge alcohol consumption interferes with the critical heart growth that occurs during adolescence.

To address this hypothesis, we utilized an outbred rat model of relatively brief (6 doses over 8 days) adolescent binge alcohol exposure. The aging period covered in this protocol (postnatal day [PND] 34–44) corresponds to a pubertal development of  $\approx$ 12 to 17 years of age in humans,<sup>17</sup> a period of rapid growth. During the protocol, control rats gavaged with tap water exhibited normal cardiac growth assessed in vivo and at the cellular level. Surprisingly, ethanol significantly impaired cardiac growth during this period and resulted in depressed ventricular filling volumes and a host of other markers of pathological stress, including inhibition of extracellular signal-related kinase (ERK1/2) physiological signaling and hyperphosphorylation of titin by PKC $\alpha$  (protein kinase C  $\alpha$ ). Interestingly, binge rats were capable of maintaining a normal cardiac output despite their smaller chamber size by increasing  $\beta$ -adrenergic stimulation. This agrees with population data that indicate high rates of binge alcohol consumption but low levels of diagnosed cardiovascular disease in adolescents. However, this compensation conceals serious underlying pathology that may sensitize the individual to additional cardiovascular disease in the future.

## METHODS

### Rat Adolescent Binge Alcohol Exposure Paradigm

The data that support the findings of this study are available from the corresponding author upon reasonable request. All animal protocols were approved by the Loyola University Chicago Institutional Animal Care and Use Committee. Male outbred Wistar rats were purchased from Charles River Laboratories and arrived in our facility at PND 25 (prepubertal). Animals were allowed to acclimate for 5 days. At PND 30, all animals were handled by the same experimenter once per day for 5 minutes to reduce nonspecific stress. The binge alcohol exposure paradigm began on PND 37. Animals were provided ad libitum access to standard rat chow and fresh tap water throughout the study.

We used a well-established physiologically relevant model of adolescent binge alcohol exposure.<sup>3</sup> First, animals were administered food-grade ethanol orally once per day at 9 AM during their normal “sleep” phase. This ensured that alcohol administration did not interfere with normal eating patterns, as evidenced by normal growth curves, and accurately modeled human teenage drinking behavior, which typically occurs late at night when they would be sleeping. Second, the dose administered follows the National Institute on Alcohol Abuse and Alcoholism definition of “binge,” which is defined as an increase in BAC to  $\geq$ 0.08 g/dL (the legal driving limit) within a 2-hour period. The calculated

BAC range at time of euthanasia (1.0 hour after oral gavage) for this model has been established as 0.08 to 0.15 for males.<sup>3</sup> Time course studies showed that the average BAC is nearly undetectable by 4.0 hours post oral gavage (Figure S1), suggesting that the animals were clinically intoxicated for a relatively short period of the 24-hour day. The model employed in these studies was a repeated binge model, designed to mimic teenage behaviors of repeated binge episodes, but not chronic addictive alcohol consumption. Therefore, animals were subjected to oral gavage of food-grade ethanol (Everclear, 190 proof, Luxco) diluted in tap water (20% volume/volume) at a dose of 3 g/kg body weight once per day for 3 consecutive days. This was followed by 2 days of water-only gavage, as would occur during intermittent periods of sobriety. Following 2 days of water only, the binge alcohol exposure was repeated once per day for 3 consecutive days and animals were euthanized 1.0 hours following the final alcohol exposure. The total number of alcohol administrations was 6x across an 8-day period.

In the first cohort of animals we examined the immediate cardiac effects of adolescent binge alcohol exposure. The animals were divided into 3 groups (Figure 1A): (1) water (n=15): tap water once per day×8 days; (2) acute binge (acute, n=8): tap water only once per day×7 days+ethanol once per day on day 8; and (3) repeated binge (binge, n=15): ethanol once per day×3 days+tap water once per day×2 days+ethanol once per day×3 days. The acute group was included to differentiate the effects of repeated binge exposure from elevated BAC levels at the time of euthanasia. Baseline echocardiography was performed on PND 34 and post-treatment on PND 44, ~55 minutes following the last gavage dose. Animals were euthanized immediately after post alcohol echocardiography, exactly 60 minutes following the last gavage.

In the second cohort, we determined the persistent cardiac effects of adolescent binge alcohol exposure. The animals were divided into water (n=9) and binge (n=11) groups as in the first cohort. Animals were

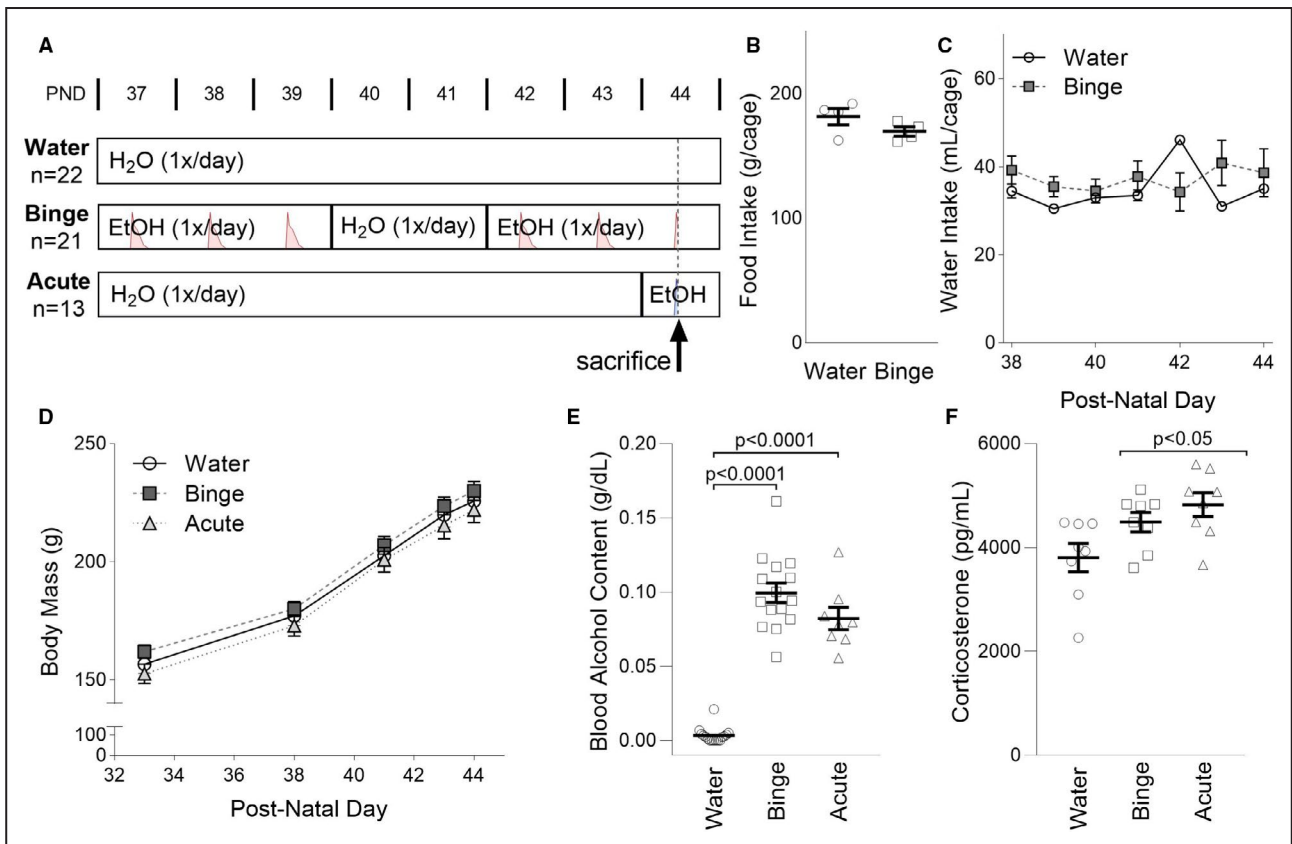


**Figure 1. Adolescent binge alcohol exposure had no effect on whole body growth.**

**A**, Binge alcohol exposure paradigm began with gavage on postnatal day (PND) 37, with outbred, male adolescent rats randomized to water, binge, and acute groups. The expected time course of blood alcohol content (BAC) for each group is shown during the protocol, with a y-axis scale of 0.10 g/dL. **B** and **C**, Food and water intake per cage (2 rats from the same treatment group per cage) was not different between the water and binge groups (n=4). **D**, All 3 groups had similar body growth over the treatment period (n=water: 20; binge: 21; acute: 8). **E**, BAC was elevated in the binge and acute groups but not the water group (n=water, 16; binge, 15; acute, 8). **F**, Corticosterone levels were elevated in the acute group (n=water: 8; binge: 8; acute: 8). Data are expressed as mean±SEM.

**Table. Functional Enrichment From RNA Sequencing Analysis of Water versus Binge**

| Biological Process (Gene Ontology) | Observed Genes, No. | False Discovery Rate |
|------------------------------------|---------------------|----------------------|
| Metabolism                         | 15                  | 0.0382               |
| Response to stress                 | 13                  | 0.0382               |
| Sarcomere structure and function   | 9                   | 0.0466               |
| Membrane transport                 | 9                   | 0.0382               |
| Regulation of growth               | 8                   | 0.0488               |
| Regulation of blood pressure       | 5                   | 0.0382               |

undisturbed following the last treatment on day 8 and were re-examined with echocardiography on PND 51.

A third cohort was necessary to determine baseline myocyte histology at pubertal onset. Animals naïve to any treatments were subjected to echocardiography and euthanized on PND 34 (BL, n=6). Histology was performed on tissue samples taken from the left ventricle to determine baseline parameters at PND 34.

### Statistical Analysis

Quantitative data were analyzed using Prism 8 (GraphPad Software). Histological images were analyzed using ImageJ (National Institutes of Health). Data were analyzed by unpaired Student *t* test, 1-way ANOVA with Tukey post hoc test, or 2-way (factors: treatment, time) repeated measures ANOVA with Sidak post hoc test, depending on the data set, as indicated in the text.  $P < 0.05$  was considered significant. PKC $\alpha$  data were inverse transformed to achieve equal variance before *t* test. The false discovery rate reported in the Table was calculated in STRING,<sup>18</sup> using a previously published approach for Multiple Testing correction.<sup>19</sup>

Further experimental procedures are presented in Data S1.

## RESULTS

### Binge Alcohol Exposure Slows Normal Cardiac Growth

There was no difference in food (Figure 1B) and water (Figure 1C) intake between the water and binge groups. The water, binge, and acute rats all grew rapidly and similarly during this period, from  $\approx 155$  g body mass to  $\approx 225$  g (Figure 1D). The binge and acute groups saw an expected rise in BAC to 0.08 g/dL (Figure 1E) and plasma corticosterone levels (Figure 1F). The BAC reached peak levels 30 to 60 minutes after gavage and fell to near zero within 4 hours (Figure S1). Thus, over the entire protocol, binge rats had BAC levels  $\geq 0.08$  for  $< 12$  total hours and detectable alcohol levels for  $\approx 24$

total hours, underscoring that this paradigm represents relatively brief overall exposure to alcohol.

To determine whether alcohol had any effects on in vivo changes in cardiac structure and function with aging in adolescent-equivalent rats, we performed echocardiography at baseline (PND 34) and post-treatment (PND 44) on all 3 groups. Example M-mode images are shown at baseline and post-treatment for the water and binge groups (Figure 2A). The water group exhibited a rapid increase in filling volume, LV end-diastolic volume (LVEDV), that was almost exactly 1:1 with the growth in body weight (Figure 2B). Unexpectedly, binge rats exhibited only half of this normal increase, so their LVEDV was significantly smaller at the end of the protocol.

Concurrently, water rats had an increase in their LV end-systolic volume (Figure 2C), such that their overall ejection fraction remained unchanged throughout the protocol (Figure 2D). The overall cardiac output increased similarly in both the water and the binge rats over the protocol (Figure 2E), suggesting that the binge rats were able to compensate for the slowed cardiac growth at a global level.

Furthermore, binge rats had a greater increase in LV posterior wall diameter than water rats (Figure 2F), indicating an accelerated hypertrophic response. However, the overall chamber diameter during diastole (summation of intraventricular septal diameter, LV interior diameter, and LV posterior wall diameter) was unchanged (Figure 2G). Together, these findings show accelerated ventricular wall growth that reduced the chamber volume rather than increased the epicardial size of the heart. There was also evidence of depressed diastolic function in vivo. Over the protocol, the water rats exhibited an increase in E/A ratio as assessed by transmitral Doppler imaging, suggesting improved diastolic function with cardiac growth, while binge rats had no such increase (Figure 2H).

There were no differences detected via echocardiography between the water and the acute groups (Figure S2), supporting that the repeated binge pattern is responsible for these effects, not the acute presence of alcohol in the system from a single binge episode.

### Binge Alcohol Alters Cellular Hypertrophy in a Regionally Specific Manner

To understand the cellular changes responsible for the LV wall hypertrophy we observed in the binge group, we performed hematoxylin and eosin histological staining to measure cardiomyocyte hypertrophy in the base, middle, and apex regions of the heart. From PND 34 (baseline) to PND 44, myocytes from both the water control and the binge groups underwent significant increases in cross-sectional area and cell length across all regions (Figure 3;  $P < 0.0001$  baseline versus

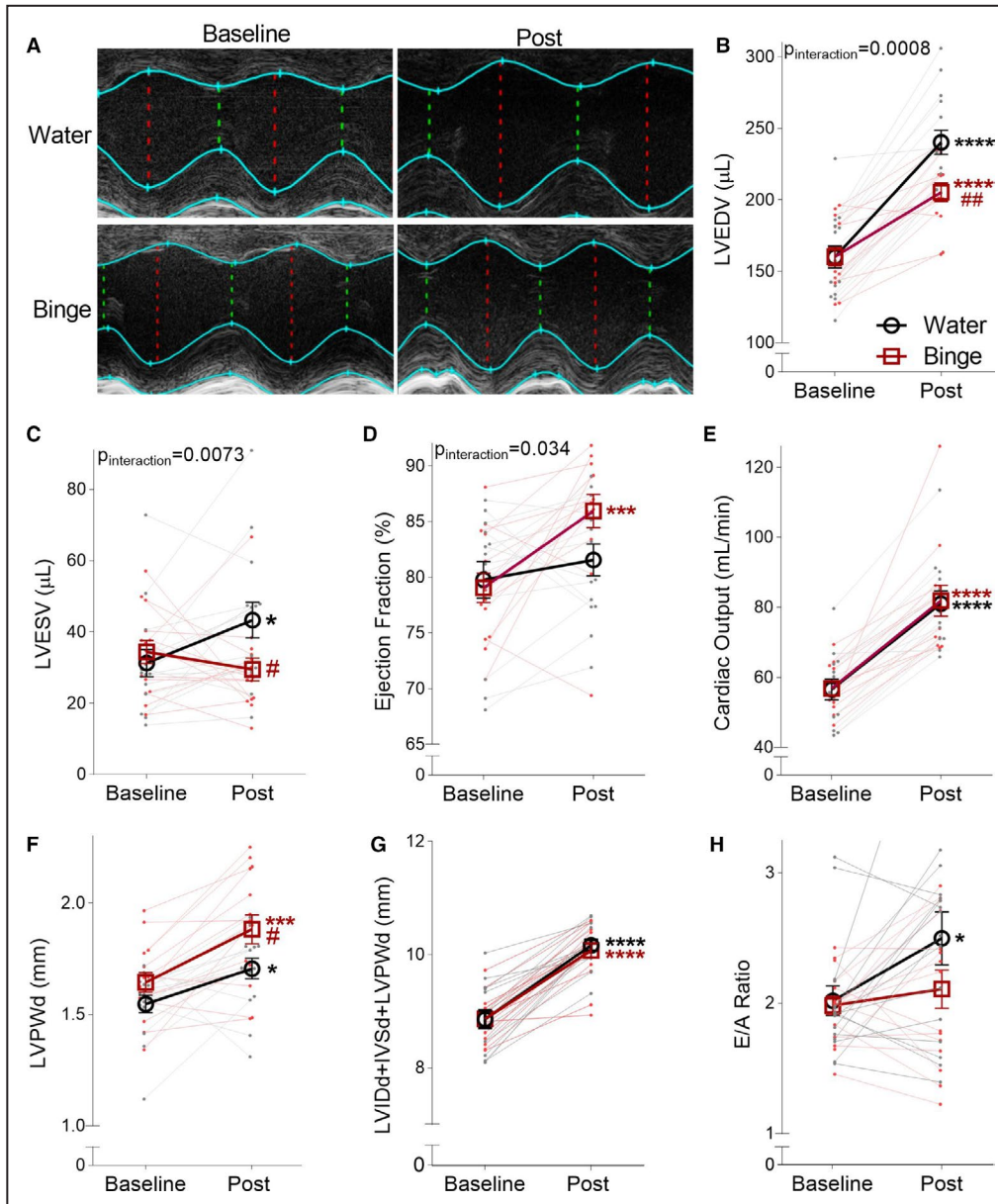


**Figure 2. Binge rats exhibited slowed cardiac growth.**

**A**, Representative M-mode echocardiography images from a water and binge rat at baseline (postnatal day [PND] 34) and post-treatment. The green dashed line represents left ventricular (LV) end-systolic diameter and the red dotted line represents LV end-diastolic diameter. **B**, Normal cardiac growth during adolescence resulted in  $\approx 65\%$  growth in left ventricular end-diastolic volume in the water group over the protocol (black open circles), but the binge rats (red open circles) had only half this increase in size. **C**, Perhaps as a compensation for this decrease in diastolic volume, the binge rats exhibited a decrease in LV end-systolic volume, compared with an increase in the water group from normal growth. **D**, Water control rats, despite normal growth, exhibited a steady ejection fraction, while binge rats experienced a significant increase. **E**, The increased systolic function in binge rats was able to compensate for the reduced filling, and cardiac output is unchanged between the groups after treatment. **F** and **G**, The binge rats had a larger LV posterior wall diameter (LVPWd) than the water rats (**F**), while overall LV dimension (**G**) was unchanged, suggesting ventricular wall hypertrophy growing inward and reducing diastolic volume. **H**, E/A ratio assessed by tissue Doppler shows an increase during normal aging in the water group that did not occur in the binge group. For B through H, n=water: 15; binge: 15. Data are expressed as mean $\pm$ SEM. \* $P < 0.05$ , \*\*\* $P < 0.001$ , \*\*\*\* $P < 0.0001$  vs baseline; # $P < 0.05$ , ## $P < 0.01$  vs water at post-treatment by 2-way repeated measures ANOVA with Sidak multiple comparisons post hoc test.

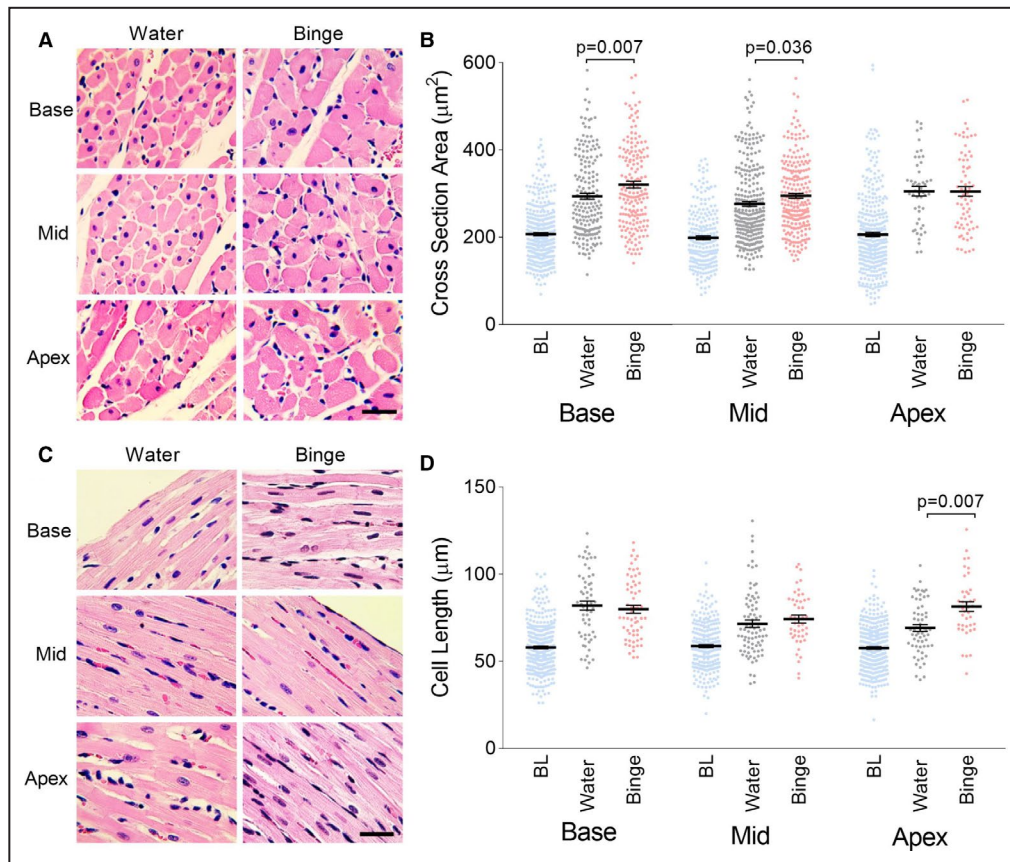


**Figure 3. Binge exposure accelerated normal cellular hypertrophy during adolescence.**

**A**, Representative hematoxylin and eosin histological images and **(B)** analysis of the water and the binge rats left ventricular (LV) cardiomyocyte cross-section areas and quantitation analysis compared with baseline rats from the base, middle, and apex. (n=base: 182–374 cells per group; middle: 239–341 cells per group; apex: 50–68 cells per group from baseline: 6 rats, water: 4 rats, binge: 4 rats). Both water and binge groups were significantly larger ( $P<0.001$ ) than baseline, from normal cellular hypertrophy, but the myocytes from binge rats grew more in the base and middle. **C**, Representative hematoxylin and eosin histological images and **(D)** analysis of the water and the binge rats LV cardiomyocyte cell lengths and the analysis compared with baseline rats at the base, middle, and apex (n=base: 58–326 cells per group; mid: 62–236 cells per group; apex: 41–321 cells per group from baseline: 6 rats, water: 4 rats, binge: 4 rats). Data are expressed as mean±SEM.

all water and binge groups, significance not indicated on figure).

Agreeing with the in vivo echocardiography data, the binge rats experienced accelerated myocyte concentric hypertrophy in the base and midwall. However, we also observed enhanced eccentric hypertrophy in the apex of binge animals.

### Myocyte Function is Depressed by Binge Alcohol Exposure

We next sought to identify the cellular mechanisms for the observed effects on in vivo cardiac function. The likely compensatory increase in systolic function observed in the binge group suggested altered contractile function at the cellular level. Myofilament force-calcium relationships were measured from individual membrane permeabilized LV myocytes from

the water and binge groups (Figure 4A). While binge alcohol exposure had no effect on maximal calcium-activated force (Figure S3) it significantly decreased calcium sensitivity in myocytes from adolescent hearts (Figure 4B).

Myofilament calcium sensitivity is regulated in part by phosphorylation of cardiac troponin I at S22/23 by PKA (protein kinase A).<sup>20</sup> We observed a ~40% increase in cardiac troponin I phosphorylation in the binge group compared with the water group (Figure 4C and 4D), explaining the observed decrease in calcium sensitivity. Phosphorylation of cardiac troponin I is a key element in the  $\beta$ -adrenergic pathway through which calcium desensitization improves myocardial relaxation. Thus, this increase in phosphorylation also suggests that the enhanced systolic function in the binge group is attributable to  $\beta$ -adrenergic signaling and activation of PKA.

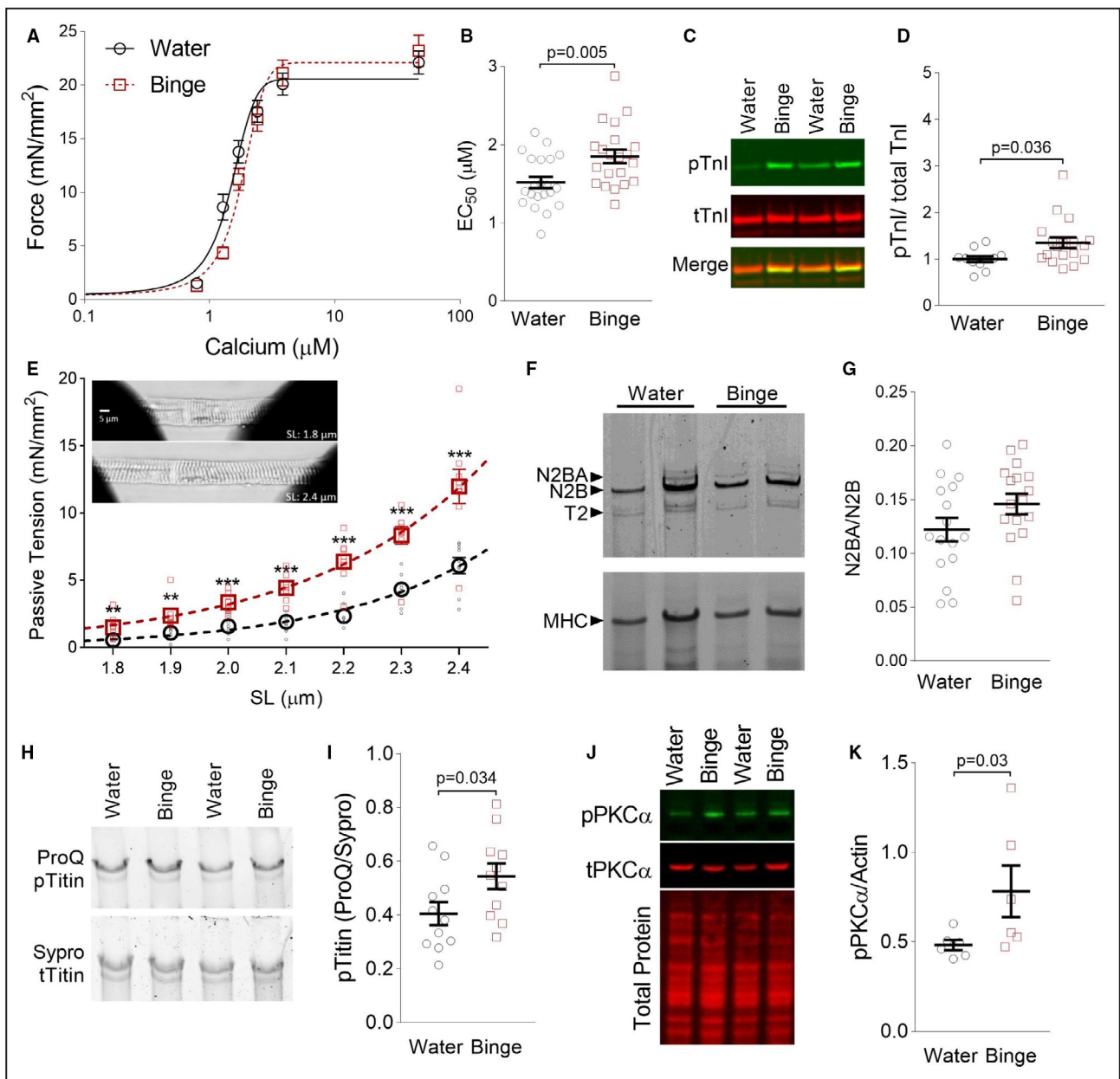


**Figure 4. Myofilament calcium sensitivity is depressed via PKA (protein kinase A) phosphorylation of troponin I.** **A**, The mean force as a function of calcium concentration and fitted curves for skinned myocytes from the water (black) and binge (red) groups. **B**, Calculated values for individual myocytes and summary values for calcium sensitivity ( $EC_{50}$ ). Binge rats exhibited a significant decrease in calcium sensitivity ( $n$ =water: 21 myocytes from 4 animals; binge: 21 myocytes from 4 animals). **C**, Representative Western blot images for total and phospho-serine 22/23 cardiac troponin I in the water, binge, and acute groups. **D**, Quantification showing an increase in cardiac troponin I PKA phosphorylation in the binge group ( $n$ =water: 11; binge: 18). Data are expressed as mean $\pm$ SEM. **E**, Single skinned myocyte passive tension generated at sarcomere lengths (SLs) between 1.8 and 2.4  $\mu$ m (with the inset showing a single cell at  $\times 40$  magnification). The binge groups showed significantly higher passive tension over all SLs, likely from changes to titin ( $n$ =water: 9 cells from 3 rats; binge: 9 cells from 3 rats [ $**P < 0.01$ ,  $***P < 0.001$  by 2-way repeated measures ANOVA with Sidak multiple comparisons post hoc test]). **F**, Example gels image showing titin isoforms and myosin heavy chain (MHC). **G**, There was no change in overall isoforms (N2BA, N2B) ( $n$ =water: 16; binge: 17). **H**, Example phosphorylation (ProQ) and total (Sypro) stained titin gel. **I**, Quantification showing an overall increase in titin phosphorylation in the binge group ( $n$ =water: 11; binge: 11). **J**, Example blot for phospho-PKC $\alpha$  (protein kinase C  $\alpha$ ) and total PKC $\alpha$ , and total protein stain. **K**, Phospho-PKC $\alpha$  normalized to actin for the water and binge groups showed an increase in active PKC $\alpha$  in the binge group ( $t$  test on transformed data,  $n$ =6 per group).

Results from tissue Doppler indicated possible impaired relaxation in the binge group. Suspecting stiffer myocardium from cardiac fibrosis, we first assessed

fibrotic area by Masson trichrome staining and observed no differences between the water and binge groups (Figure S4). Thus, we next assessed single

myocyte stiffness and found that binge myocytes had increased passive tension at every sarcomere length tested (Figure 4E).

Titin is a spring-like protein that contributes to cellular stiffness, and changes to titin isoforms or post-translational modifications can lead to increased stiffness and diastolic dysfunction.<sup>21,22</sup> We visualized the titin isoforms (the compliant N2BA isoform and the stiffer N2B isoform) and found no differences between the groups in isoform expression (Figure 4F and 4G). The binge group showed a significant reduction in the titin proteolytic cleavage product (T2) compared with the water group (Figure S5), suggesting that titin turnover and possibly sarcomere turnover were altered. However, the direction of this change cannot be inferred from the data<sup>23</sup> and does not explain the change in stiffness. Titin phosphorylation is also known to alter its stiffness, and by ProQ staining we observed an overall increase in titin phosphorylation in the binge group (Figure 4H and 4I). No differences were found in titin phosphorylation between the acute and water groups (Figure S6).

Only 2 kinases are known to phosphorylate titin and increase passive stiffness: Ca<sup>2+</sup>/calmodulin-dependent protein kinase II and PKC $\alpha$ . There was no change in total or phospho-Ca<sup>2+</sup>/calmodulin-dependent protein kinase II levels between the water and binge groups (Figure S7). However, active pS657/pY658 PKC $\alpha$  was significantly increased in the binge compared with the water rats (Figure 4J and 4K). Thus, binge alcohol

consumption increased activation of PKC $\alpha$  and titin phosphorylation, increasing cellular stiffness.

## Binge Alcohol Exposure Alters the Gene Expression Profile and Hypertrophic Signaling

One of the major nodal signaling kinases in physiological hypertrophy is ERK1/2.<sup>24</sup> The activity of ERK1/2 is controlled by its phosphorylation at Thr202/Tyr204 on ERK1 (Thr185/Tyr187 on ERK2), which were significantly decreased in the binge group compared with the water group (Figure 5A). Along with other kinases involved in physiological hypertrophy, ERK1/2 regulates downstream transcription of genes involved in growth. Thus, we next performed RNA sequencing on LV samples from 4 water and 4 binge rats. Using a cutoff of  $P < 0.05$  and  $\log(2)$  fold-change  $< -1$  or  $> 1$ , we identified 10 upregulated and 58 downregulated genes (Figure 5B, Table S1). From this data set we utilized the STRING database<sup>18</sup> to predict functionally enriched biological processes (Table). Several of these processes closely agreed with the experimental observations, such as growth, response to stress, and sarcomere structure and function. Atrial natriuretic peptide (ANP) expression was significantly downregulated in the binge rats. ANP is crucial as an inhibitor for pathological hypertrophy in adults patients with heart failure,<sup>25</sup> and it has been previously suggested that the antihypertrophic role of ANP is through activation of

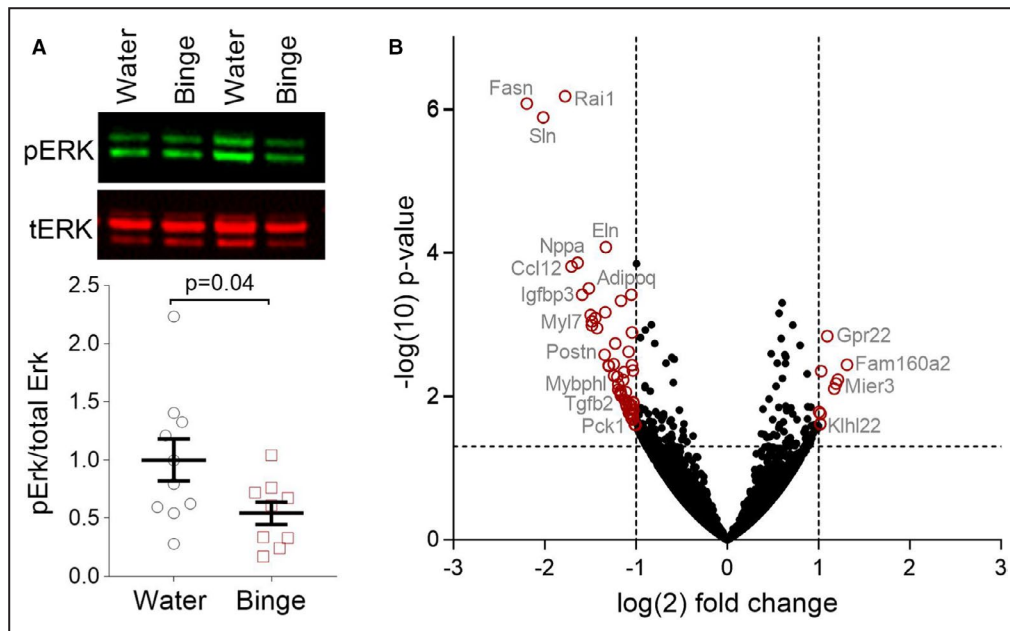


**Figure 5. Binge rats exhibited a shift in gene expression.**

**A**, Extracellular signal-related (Erk) kinase activation through phosphorylation, a central signaling kinase in physiological hypertrophy, decreased in binge rats ( $n$ =water, 10; binge, 9). **B**, Volcano plot from RNA sequencing data showing genes upregulated (10) or downregulated (58) by binge alcohol exposure in red ( $P < 0.05$  and  $\log(2)$  fold-change  $< -1$  or  $> 1$ ). A selection number of these genes are labeled.



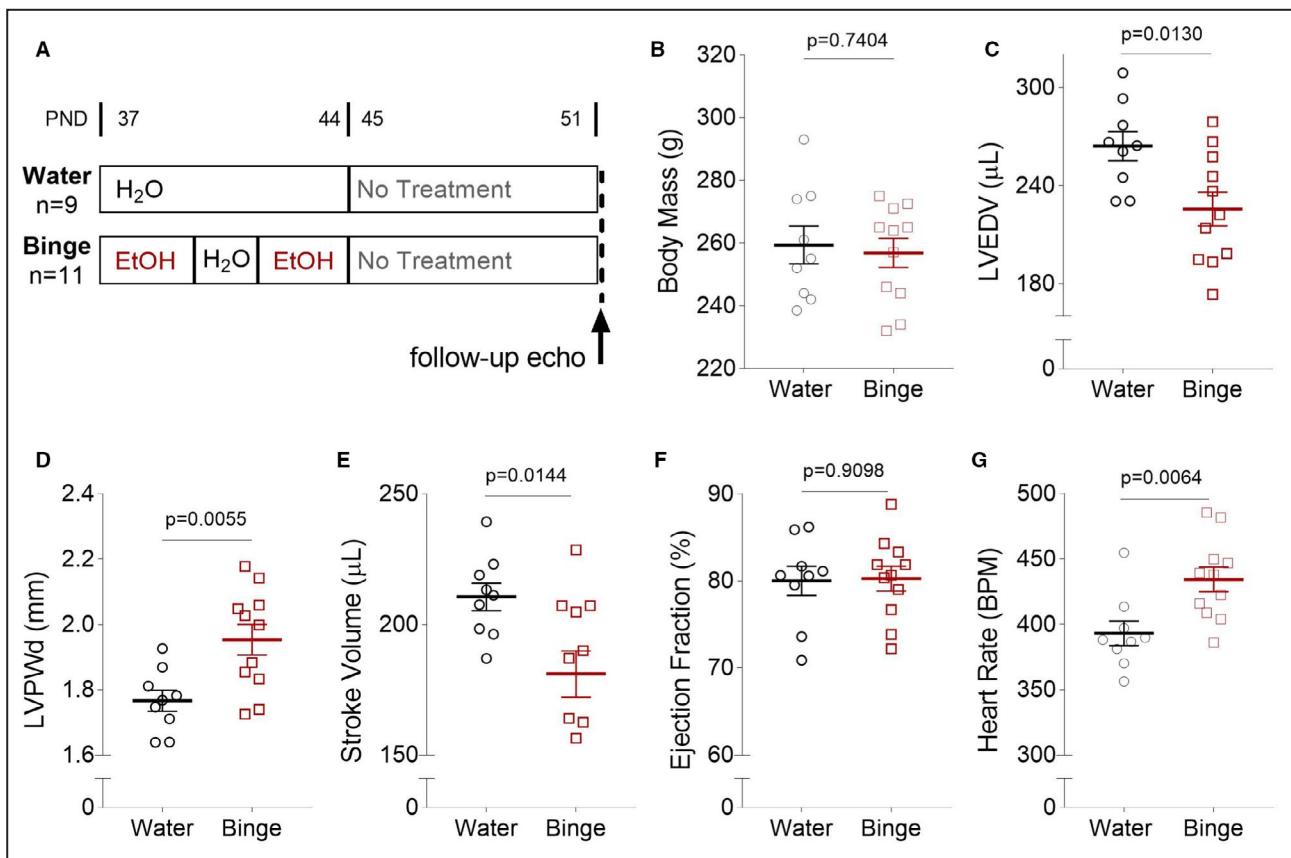


**Figure 6. The structural effects of adolescent binge alcohol persist even after the cessation of consumption.**

**A**, Rats were left undisturbed for 7 days from gavage treatment after the 8-day binge alcohol exposure paradigm. All rats had free access to pellet chow and water ad libitum. **B**, Both groups kept similar body growth post 1 week after treatment. **C through G**, Echocardiogram data comparisons between the water and the binge groups after 1 week of the cessation of binge alcohol exposure. **C**, Adolescent heart continued to grow after the 8-day paradigm, but the binge group remained to have smaller left ventricular end-diastolic volume compared with the water group. **D**, The binge group continued to have larger LV posterior wall diameter than the water group. **E**, The binge group had smaller stroke volume compared with the water group. **F**, Ejection fraction was no longer different between the binge and water groups after 1 week from binge alcohol exposure. **G**, The binge group had faster heart rates compared with the water group. n=water: 9; binge: 11. Data are expressed as mean±SEM.

ERK1/2.<sup>26</sup> These data indicate that the binge group re-oriented growth from normal physiological hypertrophy to pathological hypertrophy.

### Cardiac Structural Effects Persist After Alcohol Exposure Has Ceased

In another cohort of rats, after the end of the binge alcohol paradigm on PND44, alcohol exposure was stopped and the animals were left undisturbed until PND 51 (Figure 6A). Both water and binge rats continued to have similar whole-body growth through this follow-up period (Figure 6B). The smaller LVEDV in the binge rats persisted through adolescence after withdrawal of alcohol treatment compared with the water rats (Figure 6C), despite the cessation of alcohol exposure. Furthermore, the hypertrophied posterior wall observed immediately after treatment in the binge group also persisted (Figure 6D). In the immediate post-treatment binge rats, we observed a compensatory

increase in systolic function, which by this point was no longer present. The binge group now displayed a decrease in stroke volume compared with the water group (Figure 6E) and no change in ejection fraction (Figure 6F). However, we did observe higher heart rates during echocardiography measurements in the binge group (Figure 6G), possibly indicating persistent sympathetic stimulation to help compensate for their continued impaired growth. Thus, the effects of impaired physiological and enhanced pathologic growth persisted through adolescence even after alcohol exposure had been stopped.

## DISCUSSION

Despite high rates of teenage drinking, almost nothing is known about the cardiovascular consequences of adolescent binge alcohol consumption. Recent evidence suggests an impact on the developing brain,<sup>3</sup>

but whether there are effects on the growing heart has not previously been studied. To address this critical gap, we examined heart function in an outbred rat model of short-term adolescent binge alcohol exposure using physiologically relevant doses of food-grade alcohol delivered via gavage. We found that binge exposure significantly interfered with the normal growth process during adolescent aging. Specifically, we found that adolescent binge alcohol exposure: (1) reduced physiological growth indicated by smaller filling volumes and reduced growth signaling and gene transcription; (2) rebalanced growth towards pathological hypertrophy as shown by myocardial wall thickening and concentric cellular hypertrophy; (3) induced a compensatory increase in systolic function to maintain cardiac output likely through  $\beta$ -adrenergic activation; and (4) increased PKC $\alpha$  phosphorylation of titin leading to stiffer myocardium. Importantly, the structural consequences persisted through adolescence even after alcohol exposure had ceased. These observed effects and mechanisms may increase the individual's risk for developing heart failure as an adult (Figure 7).

These effects of binge alcohol consumption in adolescence differ in several important ways from those that have been observed in adults. First, the negative cardiovascular impact of binge alcohol at this stage of aging occurred with a much shorter period of exposure than is required in adulthood. For example, in an adult mouse model of chronic alcohol consumption there were no changes observed in heart function until

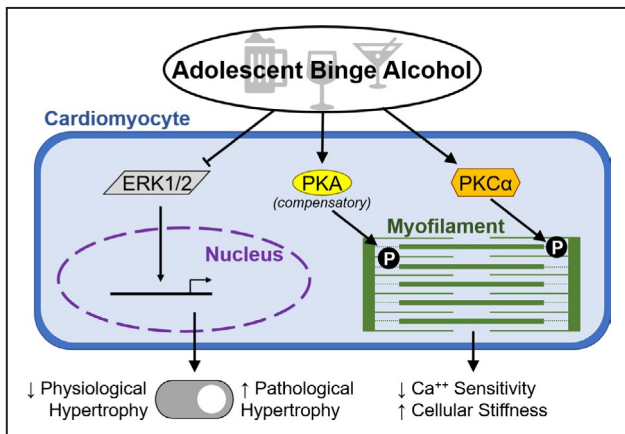


**Figure 7. Schematic of the impact of adolescent binge alcohol consumption on the heart.**

Binge alcohol inhibits extracellular signal-related kinase and atrial natriuretic peptide to switch growth from physiologic to pathologic and activates PKC $\alpha$  (protein kinase C  $\alpha$ ), leading to titin phosphorylation and increased cellular stiffness. The adolescent heart compensates for the decreased cardiac output from their smaller hearts by increasing systolic function through PKA (protein kinase A) activation, increasing phosphorylation of its targets such as troponin I, leading to myofilament calcium desensitization. The chronic consequences of hypertrophy and impaired relaxation may sensitize the adolescent for heart failure in adulthood.

40 days of exposure,<sup>13</sup> and, in humans, 20 years of follow-up showed only modest cardiac remodeling.<sup>27</sup> In adolescent-equivalent rats, just 6 doses over 8 days resulted in significant changes. The difference is likely that alcohol is both inducing cardiac dysfunction while simultaneously interfering with the normal growth process during adolescence. Further, this growth process is rapid, with rats exhibiting a 50% increase in LVEDV over this period, agreeing with human adolescent echocardiographic data showing a similar 50% increase in LVEDV during adolescence even over a wide range of baseline variability.<sup>28</sup>

Adult alcoholic cardiomyopathy patients are described as having a dilated cardiomyopathy with reduced systolic function,<sup>29</sup> although wall hypertrophy has also been described.<sup>27</sup> In the adolescent-equivalent rats, we observed a hypertrophic response and an increase in systolic function caused by upregulated  $\beta$ -adrenergic activation and PKA activity. While likely compensatory for the decreased filling volumes to maintain cardiac output,<sup>30</sup> chronic  $\beta$ -adrenergic activation is known to lead to deleterious cardiovascular effects.<sup>31,32</sup> Total abstinence can lead to reverse remodeling in adult alcoholics,<sup>33</sup> which may occur eventually here as well but not by the end period of adolescence as we have shown.

The observed changes in E/A ratio suggests impaired relaxation and increased myocardial stiffness, which further indicate diastolic dysfunction. These data agree with a study in adult humans showing that alcoholics display diastolic dysfunction (reduction in E/A ratio as well as deceleration time) compared with nonalcohol drinker controls.<sup>34</sup> Impaired relaxation is a sensitive functional indicator of alcohol abuse, and was detected in adults with a relatively short history of alcoholism (5–9 years) although longer durations of alcoholism led to more severe impairment.<sup>35</sup> Mechanistically, we also observed increases in passive tension at the cellular level. Given the short length of exposure and the slow turnover rate of titin ( $t_{1/2}$ =3.5 days<sup>36</sup>), it is not surprising that there were no changes in isoform expression as have been observed in end-stage heart failure.<sup>37,38</sup> We found hyperphosphorylation of titin in the binge group. If this was at the PKA sites (as we observed with cardiac troponin I), this increase would predict a decrease in stiffness, the opposite of what we observed. However, phosphorylation of the titin spring element PEVK at S11870 and/or S120222 by PKC $\alpha$  has been revealed to increase titin passive stiffness.<sup>39</sup> We observed an increase in PKC $\alpha$  activity with binge exposure. In fact, alcohol has previously been shown to modulate PKC $\alpha$  in a variety of tissues, although not cardiac, albeit both increases and decreases have been reported.<sup>40,41</sup> Moreover, PKC $\alpha$  is a central signaling kinase involved in a host of pathological signaling in the myocyte,<sup>42</sup> so it is likely that further

cellular dysfunction is present that we have not identified here.

We observed a decrease in ERK1/2 activation in the binge versus water rats, indicating a decrease in physiological hypertrophic signaling. In agreement with a decrease in this transcription regulation pathway, our RNA sequencing data showed mostly decreased gene expression, suggesting binge alcohol exposure is suppressing activated pathways in cardiac growth. For example, ANP,<sup>43</sup> periostin,<sup>44</sup> and insulin growth factor binding protein 3<sup>45</sup> are all reported to be increased in cardiac growth and are decreased by binge alcohol. Further, ERK1/2 phosphorylation by ANP has shown to be antihypertrophic.<sup>26</sup> These data suggest that adolescent binge alcohol exposure decreases ANP expression and may be responsible for the hypophosphorylation of ERK. The  $\beta$ -adrenergic activation by binge alcohol increased pathological wall thickness and cellular hypertrophy, and the adolescent heart lacks ANP to inhibit the effect. There were only a few upregulated genes, and these were not involved in pathological or compensatory hypertrophy pathways, further supporting that we have observed aberrant effects to normal cardiac growth rather than activated compensatory hypertrophy.

## Limitations

The adolescent heart is not as well studied as other phases across the lifespan. No longer regenerative like the immediate postnatal heart, and not as likely to develop cardiovascular disease as the adult/aging heart, cardiac growth during adolescence is comparatively less well understood. Because of this, interpreting some of our findings is challenging. For example, are there periods within adolescence where the heart is more vulnerable, such as during “growth spurts”? What are the effects of concurrent competing pathological and physiologic signaling? Ideally, future work exploring this period of critical heart growth will help us better understand the impact of stress during adolescence.

Last, these studies were performed in adolescent equivalent rats. There may be key differences in how rats and humans respond to binge alcohol in adolescence. Future studies are necessary to discover whether the findings presented here translate to human adolescents.

## CONCLUSIONS

Despite the large population of teenagers who engage in regular binge alcohol consumption and an appreciation of the effects of alcohol on the adult heart, the impact on the adolescent heart are entirely unknown. We show for the first time that binge alcohol exposure interferes with normal cardiac growth. By upregulating

$\beta$ -adrenergic stimulation, this retardation of growth could be superficially compensated for, yielding a sub-clinical pathology that would likely go unnoticed in humans. These findings agree with the population data, which, despite a high level of reported binge drinking ( $\approx 17\%$ ) indicate low levels of diagnosed cardiovascular disease in adolescents. Nonetheless, there are significant negative consequences of adolescent binge alcohol exposure, resulting in structural and functional deficits that persist even after the cessation of alcohol consumption.

## ARTICLE INFORMATION

Received December 16, 2019; accepted March 24, 2020.

### Affiliations

From the Department of Cell and Molecular Physiology, Loyola University Chicago Stritch School of Medicine, Maywood, IL (L.A., E.P., A.A., T.K., M.H., A.Z., T.R.P., J.A.K.); Department of Physiology, Wayne State University, Detroit, MI (M.A.H., C.S.C.).

### Sources of Funding

This work was funded by the National Institutes of Health (R21AA027625 and R01HL136737 to Kirk and R01AA021517 to Pak).

### Disclosures

None.

### Supplementary Materials

Data S1

Table S1

Figures S1–S7

References 46–48

## REFERENCES

- (SAMHSA) SAAHSA. 2015 national survey on drug use and health (NSDUH). 2015.
- Kann L, McManus T, Harris WA, Shanklin SL, Flint KH, Hawkins J, Queen B, Lowry R, Olsen EO, Chyen D, et al. Youth risk behavior surveillance—United States, 2015. *MMWR Surveill Summ*. 2016;65:1–174.
- Przybycien-Szymanska MM, Rao YS, Pak TR. Binge-pattern alcohol exposure during puberty induces sexually dimorphic changes in genes regulating the HPA axis. *Am J Physiol Endocrinol Metab*. 2010;298:E320–E328.
- Przybycien-Szymanska MM, Mott NN, Paul CR, Gillespie RA, Pak TR. Binge-pattern alcohol exposure during puberty induces long-term changes in HPA axis reactivity. *PLoS One*. 2011;6:e18350.
- Torcaso A, Asimes A, Meagher M, Pak TR. Adolescent binge alcohol exposure increases risk assessment behaviors in male Wistar rats after exposure to an acute psychological stressor in adulthood. *Psychoneuroendocrinology*. 2017;76:154–161.
- Asimes A, Kim CK, Cuarenta A, Auger AP, Pak TR. Binge drinking and intergenerational implications: parental preconception alcohol impacts offspring development in rats. *J Endocr Soc*. 2018;2:672–686.
- Gutgesell HP, Rembold CM. Growth of the human heart relative to body surface area. *Am J Cardiol*. 1990;65:662–668.
- Henry WL, Ware J, Gardin JM, Hepner SI, McKay J, Weiner M. Echocardiographic measurements in normal subjects. Growth-related changes that occur between infancy and early adulthood. *Circulation*. 1978;57:278–285.
- Milicević G, Narancić NS, Steiner R, Rudan P. Increase in cardiac contractility during puberty. *Coll Antropol*. 2003;27:335–341.
- Walsh S, Pontén A, Fleischmann BK, Jovinge S. Cardiomyocyte cell cycle control and growth estimation in vivo—an analysis based on cardiomyocyte nuclei. *Cardiovasc Res*. 2010;86:365–373.

11. Maresh MM. Growth of the heart related to bodily growth during childhood and adolescence. *Pediatrics*. 1948;2:382.
12. Janz KF, Dawson JD, Mahoney LT. Predicting heart growth during puberty: the Muscatine Study. *Pediatrics*. 2000;105:e63.
13. Matyas C, Varga ZV, Mukhopadhyay P, Paloczi J, Lajtos T, Erdelyi K, Nemeth BT, Nan M, Hasko G, Gao B, et al. Chronic plus binge ethanol feeding induces myocardial oxidative stress, mitochondrial and cardiovascular dysfunction, and steatosis. *Am J Physiol Heart Circ Physiol*. 2016;310:H1658–H1670.
14. Piano MR, Burke L, Kang M, Phillips SA. Effects of repeated binge drinking on blood pressure levels and other cardiovascular health metrics in young adults: National Health and Nutrition Examination Survey, 2011–2014. *J Am Heart Assoc*. 2018;7:e008733. DOI: 10.1161/JAHA.118.008733
15. Piano MR, Phillips SA. Alcoholic cardiomyopathy: pathophysiological insights. *Cardiovasc Toxicol*. 2014;14:291–308.
16. Kim SD, Beck J, Bieniarz T, Schumacher A, Piano MR. A rodent model of alcoholic heart muscle disease and its evaluation by echocardiography. *Alcohol Clin Exp Res*. 2001;25:457–463.
17. Sengupta P. The laboratory rat: relating its age with human's. *Int J Prev Med*. 2013;4:624–630.
18. Szklarczyk D, Gable AL, Lyon D, Junge A, Wyder S, Huerta-Cepas J, Simonovic M, Doncheva NT, Morris JH, Bork P, et al. STRING v11: protein-protein association networks with increased coverage, supporting functional discovery in genome-wide experimental datasets. *Nucleic Acids Res*. 2019;47:D607–D613.
19. Benjamini Y, Hochberg Y. Controlling the false discovery rate—a practical and powerful approach to multiple testing. *J R Stat Soc B*. 1995;57:289–300.
20. Layland J, Solaro RJ, Shah AM. Regulation of cardiac contractile function by troponin I phosphorylation. *Cardiovasc Res*. 2005;66:12–21.
21. Linke Wolfgang A, Hamdani N. Gigantic business titin properties and function through thick and thin. *Circ Res*. 2014;114:1052–1068.
22. LeWinter MM, Granzier H. Cardiac titin: a multifunctional giant. *Circulation*. 2010;121:2137–2145.
23. Kruger M, Kotter S. Titin, a central mediator for hypertrophic signaling, exercise-induced mechanosignaling and skeletal muscle remodeling. *Front Physiol*. 2016;7:76.
24. Mailet M, van Berlo JH, Molkentin JD. Molecular basis of physiological heart growth: fundamental concepts and new players. *Nat Rev Mol Cell Biol*. 2013;14:38–48.
25. Riegger AJG. Atrial Natriuretic Peptide in Heart Failure. In: Kaufmann W, Wambach G. (eds), *Endocrinology of the Heart*. 1989. Springer, Berlin, Heidelberg.
26. Silberbach M, Gorenc T, Hershberger RE, Stork PJ, Steyger PS, Roberts CT. Extracellular signal-regulated protein kinase activation is required for the anti-hypertrophic effect of atrial natriuretic factor in neonatal rat ventricular myocytes. *J Biol Chem*. 1999;274:24858–24864.
27. Rodrigues P, Santos-Ribeiro S, Teodoro T, Gomes FV, Leal I, Reis JP, Goff DC, Gonçalves A, Lima JAC. Association between alcohol intake and cardiac remodeling. *J Am Coll Cardiol*. 2018;72:1452–1462.
28. Pettersen MD, Du W, Skeens ME, Humes RA. Regression equations for calculation of z scores of cardiac structures in a large cohort of healthy infants, children, and adolescents: an echocardiographic study. *J Am Soc Echocardiogr*. 2008;21:922–934.
29. Urbano-Marquez A, Estruch R, Navarro-Lopez F, Grau JM, Mont L, Rubin E. The effects of alcoholism on skeletal and cardiac muscle. *N Engl J Med*. 1989;320:409–415.
30. Lymperopoulos A, Rengo G, Koch WJ. Adrenergic nervous system in heart failure: pathophysiology and therapy. *Circ Res*. 2013;113:739–753.
31. Osadchii OE. Cardiac hypertrophy induced by sustained  $\beta$ -adrenoreceptor activation: pathophysiological aspects. *Heart Fail Rev*. 2007;12:66–86.
32. Shin E, Ko KS, Rhee BD, Han J, Kim N. Different effects of prolonged  $\beta$ -adrenergic stimulation on heart and cerebral artery. *Integr Med Res*. 2014;3:204–210.
33. Izumi T, Kato H, Kodama M, Sasagawa Y, Masani F, Kodera K, Tsuda T, Shibata A, Inai T, Katsui T, et al. Cardiac involvement of alcoholics and the effect of total abstinence. *Arukoro Kenkyuto Yakubutsu Ison*. 1989;24:100–110.
34. Fernández-Solà J, Nicolás J-M, Paré J-C, Sacanella E, Fatjó F, Cofán M, Estruch R. Diastolic function impairment in alcoholics. *Alcohol Clin Exp Res*. 2000;24:1830–1835.
35. Lazarevic AM, Nakatani S, Neskovic AN, Marinkovic J, Yasumura Y, Stojicic D, Miyatake K, Bojic M, Popovic AD. Early changes in left ventricular function in chronic asymptomatic alcoholics: relation to the duration of heavy drinking. *J Am Coll Cardiol*. 2000;35:1599–1606.
36. Isaacs WB, Kim IS, Struve A, Fulton AB. Biosynthesis of titin in cultured skeletal muscle cells. *J Cell Biol*. 1989;109:2189.
37. Makarenko I, Opitz CA, Leake MC, Neagoe C, Kulke M, Gwathmey JK, del Monte F, Hajjar RJ, Linke WA. Passive stiffness changes caused by upregulation of compliant titin isoforms in human dilated cardiomyopathy hearts. *Circ Res*. 2004;95:708–716.
38. Neagoe C, Kulke M, del Monte F, Gwathmey Judith K, de Tombe Pieter P, Hajjar Roger J, Linke Wolfgang A. Titin isoform switch in ischemic human heart disease. *Circulation*. 2002;106:1333–1341.
39. Hudson B, Hidalgo C, Saripalli C, Granzier H. Hyperphosphorylation of mouse cardiac titin contributes to transverse aortic constriction-induced diastolic dysfunction. *Circ Res*. 2011;109:858–866.
40. Stubbs CD, Slater SJ. Ethanol and protein kinase C. *Alcohol Clin Exp Res*. 1999;23:1552–1560.
41. Slater SJ, Cook AC, Seiz JL, Malinowski SA, Stagliano BA, Stubbs CD. Effects of ethanol on protein kinase C  $\alpha$  activity induced by association with Rho GTPases. *Biochemistry*. 2003;42:12105–12114.
42. Marrocco V, Bogomolovas J, Ehler E, Dos Remedios CG, Yu J, Gao C, Lange S. PKC and PKN in heart disease. *J Mol Cell Cardiol*. 2019;128:212–226.
43. Klein I, Danzi S. Thyroid disease and the heart. *Circulation*. 2007;116:1725–1735.
44. Nakamura M, Sadoshima J. Mechanisms of physiological and pathological cardiac hypertrophy. *Nat Rev Cardiol*. 2018;15:387–407.
45. Surmeli-Onay O, Cindik N, Kinik ST, Ozkan S, Bayraktar N, Tokel K. The effect of corrective surgery on serum IGF-1, IGFBP-3 levels and growth in children with congenital heart disease. *J Pediatr Endocrinol Metab*. 2011;24:483–487.
46. Papadaki M, Holewinski RJ, Previs SB, Martin TG, Stachowski MJ, Li A, Blair CA, Moravec CS, Van Eyk JE, Campbell KS, et al. Diabetes with heart failure increases methylglyoxal modifications in the sarcomere, which inhibit function. *JCI Insight*. 2018;3:121264.
47. Lahmers S, Wu Y, Call DR, Labeit S, Granzier H. Developmental control of titin isoform expression and passive stiffness in fetal and neonatal myocardium. *Circ Res*. 2004;94:505–513.
48. Chung CS, Hutchinson KR, Methawasin M, Saripalli C, Smith JE III, Hidalgo CG, Luo X, Labeit S, Guo C, Granzier HL. Shortening of the elastic tandem immunoglobulin segment of titin leads to diastolic dysfunction. *Circulation*. 2013;128:19–28.

# **SUPPLEMENTAL MATERIAL**

## **Data S1. Supplemental Methods**

### *Animal Model and Tissue Preparation*

Outbred male Wistar rats (Charles River Laboratories, Wilmington, MA) arrived at our animal housing facility on post-natal day (PND) 25 and were left undisturbed for 5 days to acclimate. Rats were pair-housed within the same treatment group in environmentally controlled conditions. Rats were kept on a 12/12-hour of light /dark cycle with the lights switched on at 7 AM. Each rat was handled for 5 minutes a day between 9 AM to 10 AM from PND 30-36 to acclimate them to the handling necessary for gavage. Rats were weighed on PND 36, 38, 41, and 43 to determine the alcohol dose. Body mass was also measured on PND 44 immediately before sacrifice. Rats were sedated with 5% inhaled isoflurane and euthanized by rapid decapitation.

Water intake per cage was monitored by weighing the water bottle every other day. Food intake per cage was monitored by weighing the pellet chow before and after the 8-day alcohol treatment.

Additionally, a cohort of rats was sacrificed on PND 34 after baseline echocardiography for baseline tissue collection. Another cohort of rats were allowed to grow to assess the cardiac structure and function one week after the last treatment gavage.

### *Echocardiography*

Baseline and post-treatment echocardiography were performed on PND 34 and PND 44, respectively. Rats were sedated (2% inhaled isoflurane), and on a heated 37 °C pad to assess left ventricular (LV) chamber structure (Vevo 2100, VisualSonics; Ontario, CA). LV short axis-view was used to obtain B-mode two-dimensional images and M-mode tracings. Pulsed-wave transmitral doppler spectra of mitral inflow were recorded from an apical four-chamber view. LV chamber diameters and posterior wall thickness were measured at both systole and diastole. These parameters were used to calculate ejection fraction, both end-diastolic and end-systolic volumes, and cardiac output using the VisualSonics software.

### *Blood Alcohol Content and Corticosterone Assays*

Trunk blood from each rat was collected in heparinized tubes and centrifuged at 3,000 rpms for 10 min at 4 °C. Plasma was collected and stored at -20°. Blood alcohol content (BAC) was measured as described previously<sup>3</sup>. Briefly, BAC was measured using commercially available Alcohol Reagent Set (A750439, Pointe Scientific Inc., Canton, MI) and read at 340nm absorbance using Infinite 200 PRO (Tecan, Switzerland). Standard curves for interpolating the alcohol level of each rat were made based on dilutions using pre-measured alcohol standards (A7504-STD, Pointe Scientific Inc., Canton, MI). Plasma levels of corticosterone were measured using commercially available DetectX Corticosterone Enzyme Immunoassay Kit (K014-H1, Arbor Assays, Ann Arbor, MI) according to the manufacturer's instructions, and measured using an Infinite 200 PRO (Tecan, Switzerland) plate reader. Corticosterone levels for each rat was calculated from the raw OD using 4-parameter logistic curve (4PLC) fitting.

### *Histological Staining*

Left ventricle (LV) free wall tissue samples were dissected out and preserved in 10% formalin overnight. The tissue samples were embedded in paraffin and H&E and Mason's Trichrome staining were performed by the Histology Core at Loyola University Medical Center. Individual cardiomyocyte concentric and eccentric hypertrophy was visualized on H&E slides

under a light microscope (40X), and quantified by ImageJ software. Analysis of myocardium fibrosis was measured using ImageJ.

### *Skinned Myocyte Force Measurements*

Myocytes were prepared by homogenizing LV tissue in isolation solution with 0.3% Triton X100 and protease and phosphatase inhibitors (Thermo Fisher Scientific, Waltham, MA), as previously described<sup>46</sup>. Isolation solution consisted of (in mM): 8.91 KOH, 2 EGTA, 7.11 MgCl<sub>2</sub>, 10 Imidazole, 108.01 KCl, 5.8 ATP, 10 DTT. After skinning for 20 minutes on ice, the myocytes were washed twice and resuspended in isolation solution without Triton X100. Single myocytes were attached to a force transducer and a length controller (Aurora Scientific, Ontario, Canada), and sarcomere length (SL) was monitored using a video camera and calculated by High-Speed Video Sarcomere Length software (Aurora Scientific, Ontario, Canada). For force-calcium measures, SL was maintained at 2.1 μm and for the passive tension experiments, SL was varied from 1.8 to 2.4 μm. The temperature was kept constant at 25 °C.

The myocyte was kept in relaxing solution with phosphatase and protease inhibitors. The force was measured at various calcium concentrations by mixing Relaxing and Activating solutions in different ratios. Relaxing solution contained (in mM): 10 EGTA, 47.58 Kprop, 100 BES, 6.54 MgCl<sub>2</sub>, 6.24 ATP, 10 phosphocreatine, 10 DTT. Activation solution contained (in mM): 6.32 ATP, 6.2 MgCl<sub>2</sub>, 10 Ca<sup>2+</sup>-EGTA, 100 BES, 10 phosphocreatine, 28.12 KProp, 10 DTT, phosphatase and protease inhibitors.

Force-calcium data was fit to the Hill equation:

$$F = F_{max} \left( \frac{[Ca^{2+}]^h}{EC_{50}^h + [Ca^{2+}]^h} \right),$$

to acquire the parameters for F<sub>max</sub>, calcium sensitivity (EC<sub>50</sub>), and Hill coefficient (*h*).

### *Western Blots*

Total LV tissue lysates were separated on SDS Page Bolt 4-12% Bis-Tris plus gels (Thermo Fisher Scientific, Waltham, MA) at 180 volts for 30 minutes, and transferred to nitrocellulose membrane using a wet transfer apparatus for one hour at 10 volts (Bio-Rad Laboratories, Hercules, CA). The membrane was blocked with blocking buffer (Li-cor, Lincoln, NE) in TBS and incubated with primary antibodies overnight at 4 °C. Primary antibodies: phospho-Troponin I (1:1000, Rabbit, Cell Signaling Technology, Beverly, MA), total cardiac Troponin I (1:10,000, Mouse, IPOC inc., Ontario, Canada), phospho-ERK1/2 (1:1000, Rabbit, Cell Signaling Technology, Beverly, MA), total ERK1/2 (1:1000, Rabbit, Cell Signaling Technology, Beverly, MA), Phospho CaMKII beta + gamma + delta pThr287 Polyclonal Antibody (1:500, Rabbit, Invitrogen, Carlsbad, CA), Anti-CaMKII delta antibody [EPR13095] (1:1000, Rabbit, Abcam, Cambridge, MA), Anti-PKC alpha (phospho S657 + Y658) antibody (1:1000, Rabbit, Abcam, Cambridge, MA), and PKC alpha (H-7) (1:1000, Mouse, Santa Cruz Biotechnology, Dallas, TX). After washing 3 times in 1X TBS, blot was incubated in secondary antibodies for an hour at room temperature. Secondary antibodies (1:10000, Li-cor, Lincoln, NE): green anti-rabbit, red anti-mouse, and red anti-rabbit. Blots were imaged on (c600, Azure Biosystems, CA) and analyzed via image studio lite ver5.2 software (Li-cor, Lincoln, NE).

### *Titin Isoform Gel*

Titin isoform expression was determined using agarose gel electrophoresis as previously described<sup>47</sup>. Briefly, 10-30 mg pieces were obtained from each heart under liquid nitrogen.

Tissues were subsequently pulverized using Kontes Dounce homogenizers (Kimble Chase, Rockwood, TN) held in liquid nitrogen. Tissues were then placed at -20°C for 20 minutes to gently transition toward room temperature before solubilizing in 60°C reducing buffer (4M Urea, 1M Thiourea, 1.5% SDS, 25mM Tris-HCl adjusted to pH 6.8, 37.5mM DTT, 0.015% Brilliant Blue, 25% Glycerol, 0.004% Leupeptin, 0.02mM E-64, 0.25mM PMSF) for 20 minutes. Solubilized tissue was then centrifuged at 14.8k rpm for 5 minutes and then aliquoted, flash frozen in liquid nitrogen, and stored at -80°C. All samples were determined to be 2 mg/mL using a Lowery Assay. Each sample was loaded in 5 wells with increasing volumes in a 1% agarose (SeaKem™ Gold, Lonza Group, Switzerland) gel: 50mM Tris Base, 384mM Glycine, 0.1% SDS, 30% Glycerol, using a large-format gel system (Hoeffer SE600X, Hoefer, Inc., Holliston, MA). Gels were run at 15mA/gel for 200 minutes at 4°C and then stained with Coomassie Brilliant Blue. Gels were scanned using a commercially available scanner (Epson V850, Epson America, Inc., Long Beach, CA) with a calibrated Optical Density step tablet. The scan was normalized for Optical Density using a custom MATLAB script (Mathworks, Natick MA) and analyzed using ImageQuant TL (GE Healthcare Bio-Sciences Corp., Marlborough, MA) with a manual baseline subtraction. Ratios of N2BA/N2B, T2/TTN, and TTN/MHC were calculated and recorded.

### *Titin Phosphorylation*

Total phosphorylation of Titin and Myosin Heavy Chain (MHC) was determined using Pro-Q Diamond staining as previously described<sup>48</sup>. Briefly, custom 2-12% gradient acrylamide gels (2 or 12% Acrylamide, (1:50) Bis-acrylamide, 0.1% SDS, 5% glycerol, 10x Fairbanks buffer (400mM Tris Base, 200mM Sodium Acetate, 20mM EDTA, pH adjusted to 7.5 with glacial acetic acid), 0.0625% Ammonium Persulfate, and 0.0875% TEMED) were prepared and polymerized in a Mini-PROTEAN Cassettes (Bio-Rad Laboratories, Hercules, CA). Electrophoresis was pre-run with running buffer (10x Fairbanks buffer, 0.1% SDS, and 11.44mM  $\beta$ ME) at 60V for 3 minutes without sample. Solubilized samples were then loaded and gel electrophoresed first at 60V for 68 minutes, then at 90V for 70 minutes. Gels were fixed overnight in 50% methanol and 10% acetic acid, washed three times using ultrapure water (18.2 M $\Omega$ •cm), and stained for total phosphate content using a rapid protocol for Pro-Q Diamond staining (Thermo Fisher Scientific, Waltham, MA). Gels were subsequently destained using Pro-Q Diamond Destain Solution and washed twice with ultrapure water before scanning with a Typhoon Trio+ scanner (GE Healthcare Bio-Sciences Corp., Marlborough, MA) at 532-nm excitation and 560-nm emission. Gels were then stained for total protein content with Sypro Ruby Gel Stain using a rapid protocol (Thermo Fisher Scientific, Waltham, MA), washed, and scanned with a Typhoon Trio+ scanner at 488-nm excitation and 610-nm emission. Pro-Q Diamond and Sypro Ruby fluorescence was quantified using ImageQuant TL (GE Healthcare Bio-Sciences Corp, Marlborough, MA). The ratio between Pro-Q and Sypro fluorescence is reported.

### *RNA Extraction and Sequencing*

LV free wall tissue (30-60 mg) was used for total RNA extraction. RNA was isolated using RNeasy plus mini kit (74134, Qiagen, Germany) according to the manufacturer's instructions. Isolated RNA concentration in each sample was measured using NanoDrop OneC (Thermo Fisher Scientific, Waltham, MA). Illumina RNA sequencing was performed with total RNA ( $n$ : Water = 4; Binge = 4) at University of Chicago Genomics Facility. Primary data were



transferred to Galaxyproject.org and analyzed with FastQC for quality control. Low quality base reading data were filtered by Trimmomatic. All readings were consensus with rat genome aligned using HISAT2, followed by FeatureCounts analyses. Gene fold change and dispersion were measured using DEseq2. STRING website was used for biological pathways and function searches of each gene.

**Table S1. Gene Expression Changes with Binge Alcohol Exposure.**

| <b>Gene</b>      | <b>Protein</b>                                      | <b>log(2)<br/>FC</b> | <b>-log10 p-<br/>value</b> |
|------------------|---|----------------------|----------------------------|
| <b>Fasn</b>      | Fatty Acid Synthase                                 | -2.20                | 6.07                       |
| <b>Sln</b>       | Sarcosine   | -2.02                | 5.88                       |
| <b>Rai1</b>      | Retinoic acid-induced protein 1                     | -1.78                | 6.17                       |
| <b>Ccl12</b>     | Chemokine ligand 12                                 | -1.71                | 3.81                       |
| <b>Fchsd1</b>    | FCH and double SH3 domains protein 1                | -1.64                | 3.86                       |
| <b>Nppa</b>      | Atrial natriuretic peptide                          | -1.59                | 3.41                       |
| <b>C1rl</b>      | Complement C1r subcomponent                         | -1.52                | 3.50                       |
| <b>Pold2</b>     | DNA polymerase delta subunit 2                      | -1.50                | 3.13                       |
| <b>Rce1</b>      | CAAX prenyl protease 2                              | -1.48                | 3.04                       |
| <b>Myl7</b>      | Myosin regulatory light chain 2, atrial             | -1.48                | 2.98                       |
| <b>Igf3</b>      | Insulin growth factor binding protein 3             | -1.45                | 3.09                       |
| <b>Trpv6</b>     | Transient receptor potential channel V6             | -1.43                | 2.95                       |
| <b>Postn</b>     | Periostin   | -1.35                | 2.58                       |
| <b>Inpp5d</b>    | Phosphatidylinositol 3,4,5-triphosphate phosphatase | -1.34                | 3.17                       |
| <b>Eln</b>       | Elastin   | -1.33                | 4.08                       |
| <b>Hamp</b>      | Hepcidin  | -1.30                | 2.43                       |
| <b>Bmp10</b>     | Bone morphogenetic protein 10                       | -1.30                | 2.42                       |
| <b>Ptx3</b>      | Pentraxin 3   | -1.25                | 2.45                       |
| <b>Sept5</b>     | Septin-5  | -1.24                | 2.28                       |
| <b>Fxyd3</b>     | FXD domain-containing ion transport 3               | -1.23                | 2.73                       |
| <b>Adipoq</b>    | Adiponectin   | -1.20                | 2.27                       |
| <b>Bbs4</b>      | Bardet-Biedl syndrome 4                             | -1.20                | 2.16                       |
| <b>Lrrc8c</b>    | Leucine-rich repeat-containing 8c                   | -1.19                | 2.09                       |
| <b>Wsb1</b>      | WD repeat and SOCS box containing 1                 | -1.17                | 2.07                       |
| <b>Dis3l</b>     | Dis3-like exonuclease                               | -1.17                | 2.05                       |
| <b>Mepe</b>      | Matrix extracellular phosphoglycoprotein            | -1.17                | 2.00                       |
| <b>Scn7a</b>     | Sodium channel protein type 7 a                     | -1.17                | 2.02                       |
| <b>Mybph</b>     | Myosin binding protein H                            | -1.17                | 3.33                       |
| <b>Scd1</b>      | Acyl-CoA desaturase 1                               | -1.14                | 2.23                       |
| <b>Nudt6</b>     | Nucleoside diphosphate-linked moiety X6             | -1.13                | 2.34                       |
| <b>Mybphl</b>    | Myosin binding protein H like                       | -1.12                | 1.95                       |
| <b>Egfl7</b>     | EGF-like domain 7                                   | -1.11                | 2.06                       |
| <b>Sbk2</b>      | Serine/threonine kinase SBK2                        | -1.11                | 1.89                       |
| <b>Tkt</b>       | Transketolase                                       | -1.10                | 1.86                       |
| <b>H2afy2</b>    | H2A histone family                                  | -1.08                | 2.62                       |
| <b>LOC500227</b> | RIKEN cDNA  | -1.08                | 1.77                       |
| <b>Zfx2</b>      | Zinc finger homeobox protein 2                      | -1.08                | 1.77                       |

|                   |  |       |      |
|-------------------|--|-------|------|
| <b>Nap115</b>     | Nucleosome assembly protein 1                      | -1.07 | 1.87 |
| <b>Cnm2</b>       | Metal transporter, divalent metal (Mg>Co>Mn>Sr...) | -1.07 | 1.76 |
| <b>RGD1307155</b> | UPF0585 protein                                    | -1.06 | 1.75 |
| <b>Pck1</b>       | Phosphoenolpyruvate carboxykinase                  | -1.06 | 1.88 |
| <b>Tgfb2</b>      | Transforming Growth Factor beta-2                  | -1.05 | 1.74 |
| <b>Lypd1</b>      | Ly6/PLAUR domain containing 1                      | -1.05 | 3.41 |
| <b>Ednra</b>      | Endothelin-1 receptor                              | -1.05 | 1.81 |
| <b>Tusc5</b>      | Tumor supressor candidate 5 homolog                | -1.05 | 1.74 |
| <b>Zfp644</b>     | Zinc finger protein 644                            | -1.05 | 1.69 |
| <b>Lrrc61</b>     | Leucine-rich repeat-containing 61                  | -1.05 | 2.89 |
| <b>Rel2</b>       | RELT-like protein 2                                | -1.04 | 2.43 |
| <b>Rab15</b>      | Ras related protein, Rab-15                        | -1.04 | 1.73 |
| <b>Stard10</b>    | PCTP-like protein                                  | -1.04 | 1.67 |
| <b>Psip1</b>      | pC4 and SFRS1-interacting protein                  | -1.03 | 2.36 |
| <b>Tmem119</b>    | Transmembrane protein 119                          | -1.03 | 1.92 |
| <b>Car3</b>       | Carbonic anhydrase 3                               | -1.03 | 1.92 |
| <b>Sncg</b>       | Gamma synuclein                                    | -1.03 | 1.90 |
| <b>Arhgap25</b>   | Rho GTPase-activating protein 25                   | -1.03 | 1.81 |
| <b>Hps3</b>       | Hermansky-Pudlak syndrome 3                        | -1.02 | 1.88 |
| <b>Plekha4</b>    | Pleckstrin homology domain containing A4           | -1.01 | 1.61 |
| <b>Tnip2</b>      | TNFAIP3-interacting protein                        | -1.00 | 1.60 |
| <b>Dgkb</b>       | Diacylglycerol kinase beta                         | 1.01  | 1.78 |
| <b>Gars</b>       | Glycine - tRNA ligase                              | 1.02  | 1.61 |
| <b>Rprd1b</b>     | Regulation of nuclear pre-mRNA 1b                  | 1.02  | 1.62 |
| <b>Klhl22</b>     | Kelch-like protein 22                              | 1.02  | 1.76 |
| <b>Gbas</b>       | Protein NipSnap homolog 2                          | 1.03  | 2.35 |
| <b>Gpr22</b>      | G-protein coupled receptor 22                      | 1.10  | 2.84 |
| <b>Racgap1</b>    | Rac GTPase activating protein 1                    | 1.17  | 2.10 |
| <b>Dars2</b>      | Aspartate tRNA ligase                              | 1.19  | 2.18 |
| <b>Mier3</b>      | Mesoderm induction early response 3                | 1.21  | 2.23 |
| <b>Fam160a2</b>   | FTS and Hook interacting protein (FHIP)            | 1.31  | 2.44 |

## Supplemental Figures

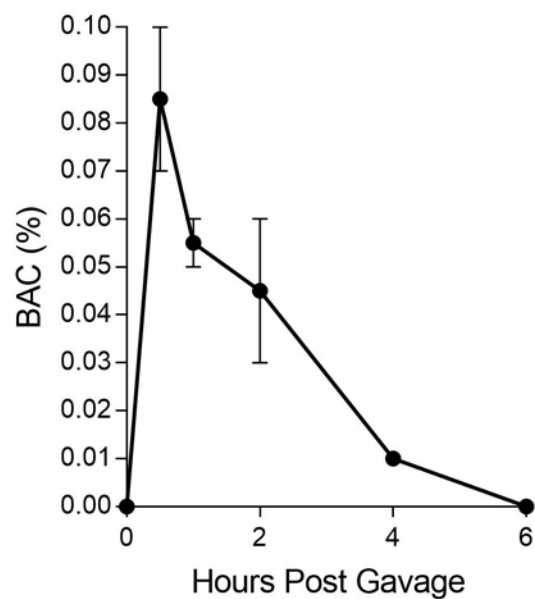


**Figure S1. Time Course of BAC after Alcohol Gavage.** Blood alcohol content levels in rats measured at 0.5, 1, 2, 4, and 6 hours after ethanol gavage. Within two hours the rats reach 0.08% (definition of binge alcohol consumption). By 4 hours post gavage, blood alcohol content is negligible. Data are  $n = 2-3$  rats per time point.

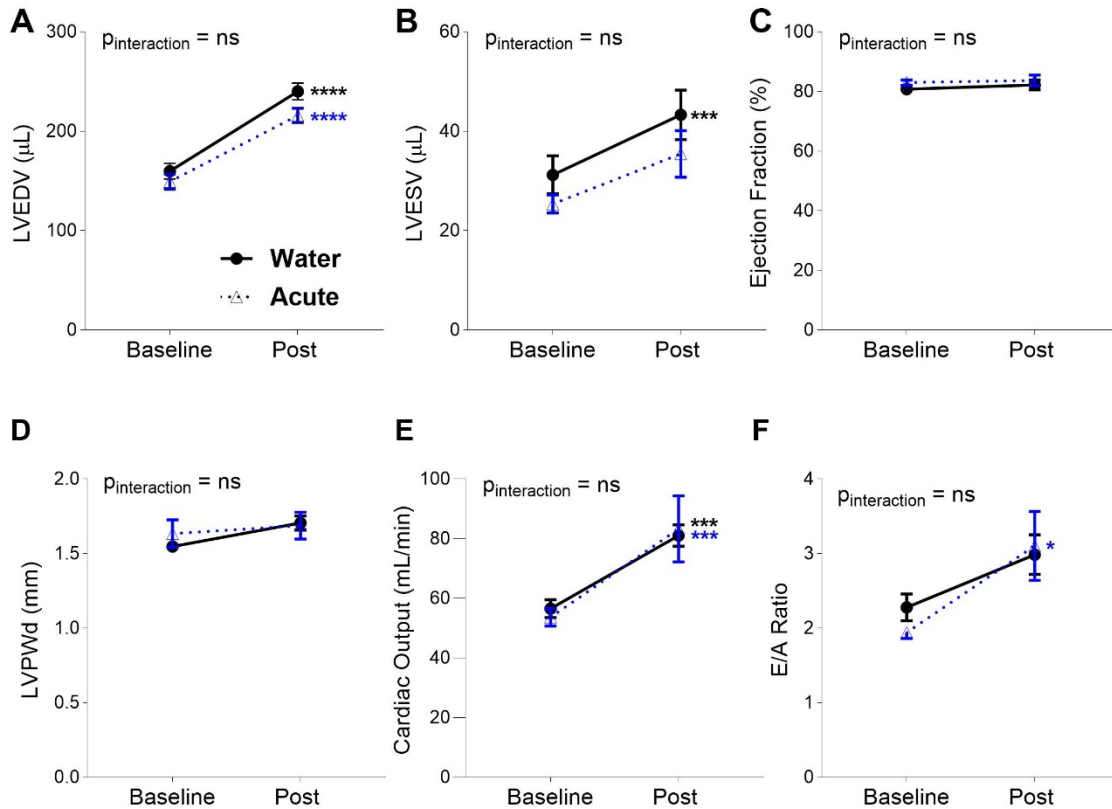


**Figure S2. No Differences between the Water and Acute Groups on Echocardiogram.** (A, B) Both the Water and the Acute groups had similar LV end-diastolic volume (LVEDV) and LV end-systolic volume (LVESV) increase. (C) Both the Water and the Acute groups maintained similar ejection fraction. (D, E) Both the Water and the Acute groups had similar LV posterior wall thickness during diastole (LVPWd) and cardiac output increase. (F) Two groups had similar E/A ratios. *n*: Water = 15, Acute = 8. Data are mean  $\pm$  SEM. \* $p < 0.05$ , \*\*\* $p < 0.001$ , \*\*\*\* $p < 0.0001$  vs. baseline; by two-way repeated measures ANOVA with Sidak's multiple comparisons post hoc test.

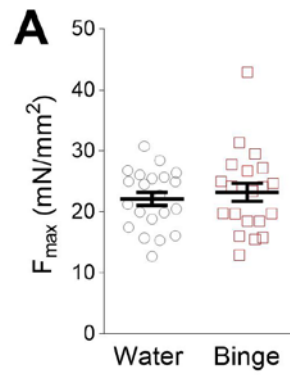


**Figure S3. Maximal Calcium Activated Force Remained the Same between Two Groups.** (A) Both the Water and the Binge groups generated similar myocyte myofilament maximal calcium activated force ( $F_{\max}$ ). ( $n$ : Water = 4, Binge = 4; 5-6 cells per animal). Data are mean  $\pm$  SEM. Statistics by unpaired student's t-test.

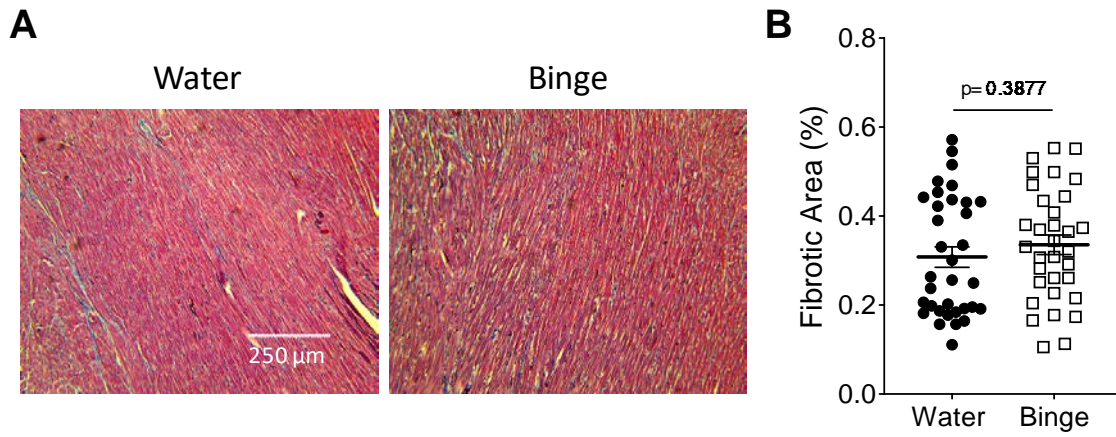


**Figure S4. Binge Alcohol Exposure Had No Effect on Myocardial Fibrosis.** (A) Representative Masson's Trichrome staining images of the Water and the Binge groups. (B) Quantification of the fibrotic area per histology image. *n*: Water = 34 images from 4 rats, Binge = 33 images from 4 rats. Data are mean  $\pm$  SEM. Statistics by unpaired student's t-test.

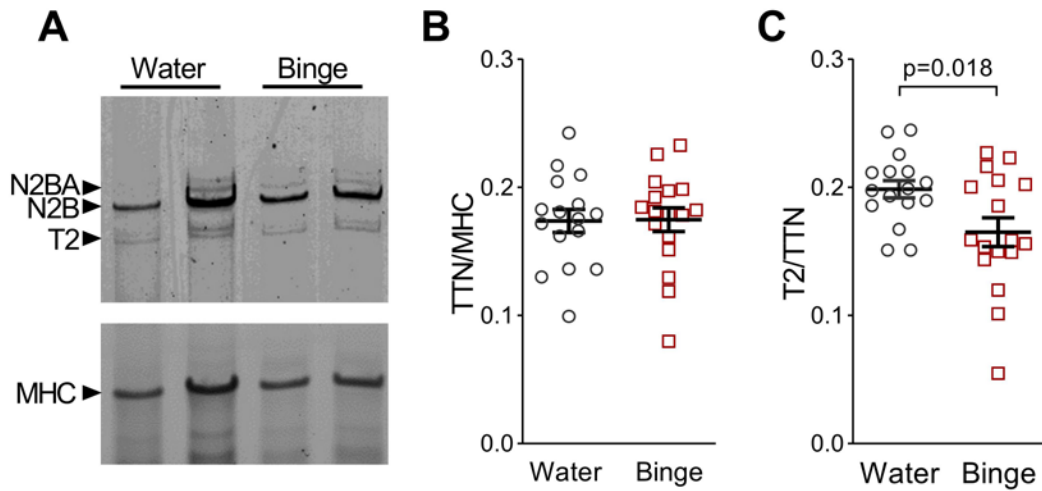


**Figure S5. Titin Expression and Proteolytic Cleavage in the Binge Group.** (A) Example gels image showing titin isoforms and myosin heavy chain (MHC). (B) There was no change overall titin (TTN) expression comparing to myosin heavy chain (MHC). (C) Binge group had significant lower titin proteolytic cleavage product (T2) expression ( $n$ : Water = 16, Binge = 17). Statistics by unpaired student's t-test.



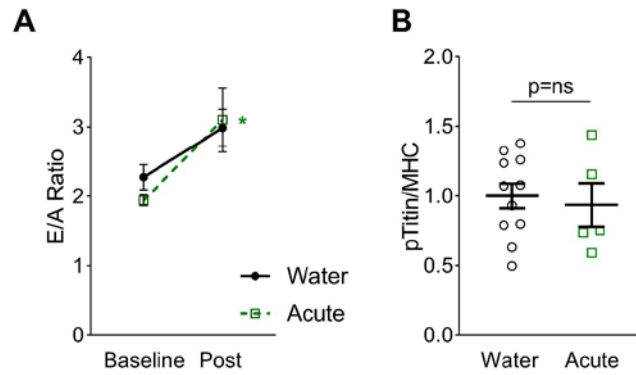


**Figure S6. No Differences in E/A Ratio or Titin Phosphorylation between the Water and Acute Groups.** (A) No difference in E/A ratio was observed between the Water and the Acute groups at post treatment.  $n$ : Water = 8, Acute = 8. (B) Both the Water and the Acute groups have similar total titin phosphorylation compared to MHC control.  $n$ : Water = 11, Acute = 5. All data mean  $\pm$  SEM.  $p_{\text{interaction}}=\text{ns}$ ,  $p_{\text{source of variance: time}}=0.0057$ . \* $p<0.05$  Acute post treatment vs. baseline, repeated measure two-way ANOVA with Sidak's post hoc test for (A); unpaired t-test for (B).

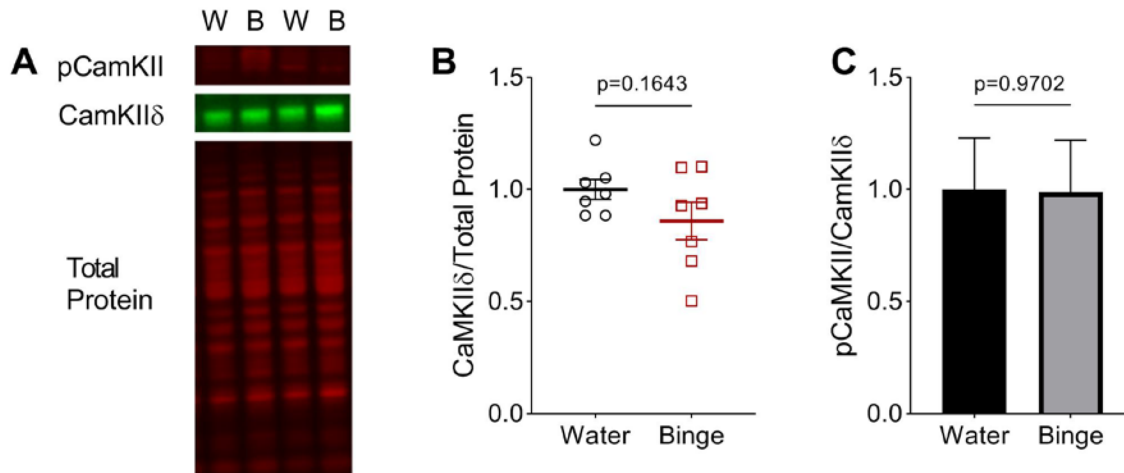


**Figure S7. No Differences in CaMKIIδ or Phosphorylated CaMKII between Water and Binge Groups.** (A) Representative western blot images for phosphorylated CaMKII, CaMKIIδ, and total protein in Water and Binge groups. (B) Quantification showing no difference in CaMKIIδ expression between two groups ( $n$ : Water = 7, Binge = 7). (C) Quantification showing no difference in phospho CaMKII to CaMKIIδ ratio between two groups ( $n$ : Water = 7, Binge = 7). Data are mean  $\pm$  SEM; by unpaired student's t-test.